Bulletin of Earthquake Engineering
https://doi.org/10.1007/s10518-026-02371-6

ORIGINAL ARTICLE

Sensitivity of urban seismic damage predictions to input data detail: an application to Sanremo, Italy

Margherita Gabriella Bruna Merani[1] · **Daniele Sivori**[1,3] · **Sergio Lagomarsino**[1] · **Simone Barani**[2] · **Serena Cattari**[1]

Received: 5 August 2025 / Accepted: 15 January 2026

Abstract
The accuracy of seismic damage scenarios is of paramount relevance for various objectives inherent to disaster risk management and particularly critical to support effective emergency response and to address seismic mitigation policies. When transitioning from large-scale studies – such as national ones – to urban scale applications, the assessment does not often reflect a downscaling in the detail level of exposure, vulnerability, and hazard data, leading to inaccurate evaluations of damage and loss, as well as of the related uncertainty. While the value of local, high-resolution data is widely acknowledged, its quantitative impact on final damage predictions remains poorly constrained. This study addresses this gap by quantifying the sensitivity of urban damage predictions to varying levels of detail in hazard, vulnerability, and exposure data. Specifically, the study compares estimates derived from large-scale datasets against those based on refined, local information acquired on-site. To this aim, a multi-level comparative framework is applied to the Sanremo Municipality (Northwestern Italy), simulating ground-motion scenarios consistent with the 1887 M6.3 Ligurian Sea earthquake. Within this framework, ground shaking is estimated using ground-motion prediction equations, which are amended to account for site-specific amplification effects. This critical step compares results derived from national soil classification maps against detailed seismic microzonation studies. Building damage and consequences are then assessed using fragility curves. Outcomes from vulnerability models based on standard aggregated census-level data are compared to those derived from refined inventories and field inspections. The results show substantial discrepancies between the predicted scenarios. The use of local data, particularly site-specific amplification effects and building characteristics, leads to significant differences in damage intensity and, especially, its spatial distribution. This study underscores the critical importance of improving knowledge through acquisition of local data and provides a robust general framework to improve decision-making for disaster risk management.

Keywords Risk assessment · Seismic vulnerability · Damage scenarios · Fragility curves · Site amplification

Extended author information available on the last page of the article

Published online: 30 January 2026

1 Introduction

Urban areas, as centres of human and economic activity, constitute contexts of potentially high risk when subjected to seismic hazard (Bilham 2009; Alexander, D. E., 2010; Brunelli et al. 2022), highlighting the need for effective disaster risk management procedures. In fact, while preventive risk assessment – ranging from national evaluations (Dolce et al. 2021) to detailed urban and building-specific studies (e.g., Vicente et al. 2011; Ferreira et al. 2017; Chieffo et al. 2021) – is fundamental, the need for tools that can rapidly and reliably estimate damage scenarios and expected consequences in the immediate post-earthquake emergency phase is equally crucial (Li et al. 2024; Zhang et al. 2025).

In the last decades, advancements in scientific research and technological innovation have significantly improved seismic risk assessment. The integration of large-scale predictive models, high computational capabilities, and Geographic Information System (GIS) platforms (Ilic et al. 2020) has enhanced our ability to analyze seismic events. Rapid seismic shaking estimation tools, such as ShakeMap (Wald et al. 1999), provide regional intensity maps that feed into platforms like HAZUS (Kircher et al. 2006), OpenQuake (Silva et al. 2014), or national tools such as IRMA (Italian Risk Maps) in Italy (Borzi et al., 2021), where shaking data is integrated with detailed inventories of exposed assets and their structural vulnerabilities. By applying fragility and consequence functions, these tools generate scenarios of expected physical damage, economic losses, and population impacts, thereby supporting critical situational awareness for risk managers.

However, while extremely powerful for providing a regional overview of seismic risk distribution, tools operating on a national scale struggle to represent the fine-grained spatial variability of urbanized contexts. Downscaling the risk assessment requires, in fact, to increase the data detail to maintain accuracy. Despite that, models developed for national and regional scales are often adopted at smaller scales with significant limitations. Primarily, they may fail to capture local modification of seismic shaking produced by the actual geological and geotechnical subsurface conditions, which regional maps only represent coarsely. Furthermore, these tools face challenges in accurately representing the heterogeneity vulnerability of the urban building stock, as its seismic response often deviates from predictions based on coarse structural information derived from census surveys – such as those conducted by ISTAT (the Italian National Institute of Statistics). Therefore, addressing the complexities related to the scale of analysis is fundamental to develop reliable damage scenarios at the urban scale and requires more targeted approaches.

The primary objective of the present study is to systematically investigate and quantify how the level of detail in input data influences seismic damage scenarios. Rather than proposing a new methodology, this work applies a multi-scale framework to show how the synergistic integration of information with varying levels of detail significantly influences the resulting damage scenarios. Unlike national evaluations, this study focuses on urban-scale damage predictions, illustrating that local assessments require a level of data detail far greater than that used in national applications. To effectively transition between the two scales, input data must be consistent with the desired resolution of the output.

Specifically, the research explores the variation in the level of detail in the input data for seismic hazard, exposure, and vulnerability. For seismic hazard, the influence of different amplification factors is considered: this includes simplified approaches, such as those based on the well-known $V_{s,30}$ parameter, as well as more detailed local seismic hazard informa-

tion captured by Seismic Microzonation (MS) studies. Concerning exposure, the analysis encompasses a spectrum of data granularity, from aggregated ISTAT census data to highly detailed building-by-building inventories. These data were complemented by accurate building vulnerability information obtained, for example, from rapid survey methodologies like the CARTIS form (Zuccaro et al. 2023), or from simplified engineering analyses, including those for determining the Emergency Limit Condition (ELC) within the framework of MS studies according to national standards (Dolce et al. 2018). Numerous Italian (e.g., Brando et al. 2021) and international (e.g., Ferreira et al. 2017) studies document the application of detailed data for vulnerability and risk assessment on the urban scale. In this study, while recognizing that the compilation of building-by-building data can be time-consuming, even with the aid of recent machine learning approaches for building characterization (e.g., Carpanese and Donà 2023; Tocchi et al. 2023; Gouveia et al. 2024), detailed datasets were elaborated and employed to fully understand their impact on seismic scenarios. For vulnerability, the analysis incorporates various fragility models, comparing results from national-level models against locally calibrated structural vulnerability models derived from fragility functions informed by ISTAT census data, CARTIS surveys, and in-situ inspections.

The comparative framework is applied to the municipality of Sanremo (IM, Italy) as a pilot case study. Sanremo was chosen as a representative example of a medium-sized coastal city with typological diversity, socio-economic relevance (Cattari et al. 2024), and, crucially, the availability of the necessary pre-existing detailed datasets (MS, CARTIS, and ELC data) needed to perform the sensitivity analysis. Furthermore, the city is characterized by historical seismicity, as it was struck by the 1887 Ligurian Sea earthquake, an event with an estimated magnitude of 6.3, which caused more than 600 deaths and severe damage.

The paper is organized as follows. Section 2 presents the comparative framework and the components of the methodology developed for predicting damage scenarios, with regard to both urban-scale ground shaking estimation and building-scale vulnerability and damage evaluation. Section 3 establishes the context for the case study, the municipality of Sanremo, briefly describing the seismological and geological conditions, and the specific features of its building inventory, which are influenced by historical construction practices. Section 4 delves into the methodological components, detailing the generation of ground shaking estimates under various site amplification assumptions and discussing the selection, comparison, and local adaptation of building fragility models according to detailed survey data. Section 5 discusses the results, presenting the damage scenarios for Sanremo, analysing the sensitivity of outcomes to different exposure data and modeling choices, and estimating potential consequences on buildings. Finally, the last section evaluates the strengths and limitations of the proposed approach and identifies potential future developments of our tool in supporting emergency management decisions.

2 Methodological framework for rapid seismic damage estimation

The methodological framework adopted in this study to systematically assess the impact of data detail integrates analyses across both urban and building scales. The overall process follows a sequence of steps (Fig. 1) designed to combine rapid ground-motion assessment with detailed vulnerability models to enable timely damage prediction. This framework is not presented as a novel methodology, but rather as a structured approach for quantify-

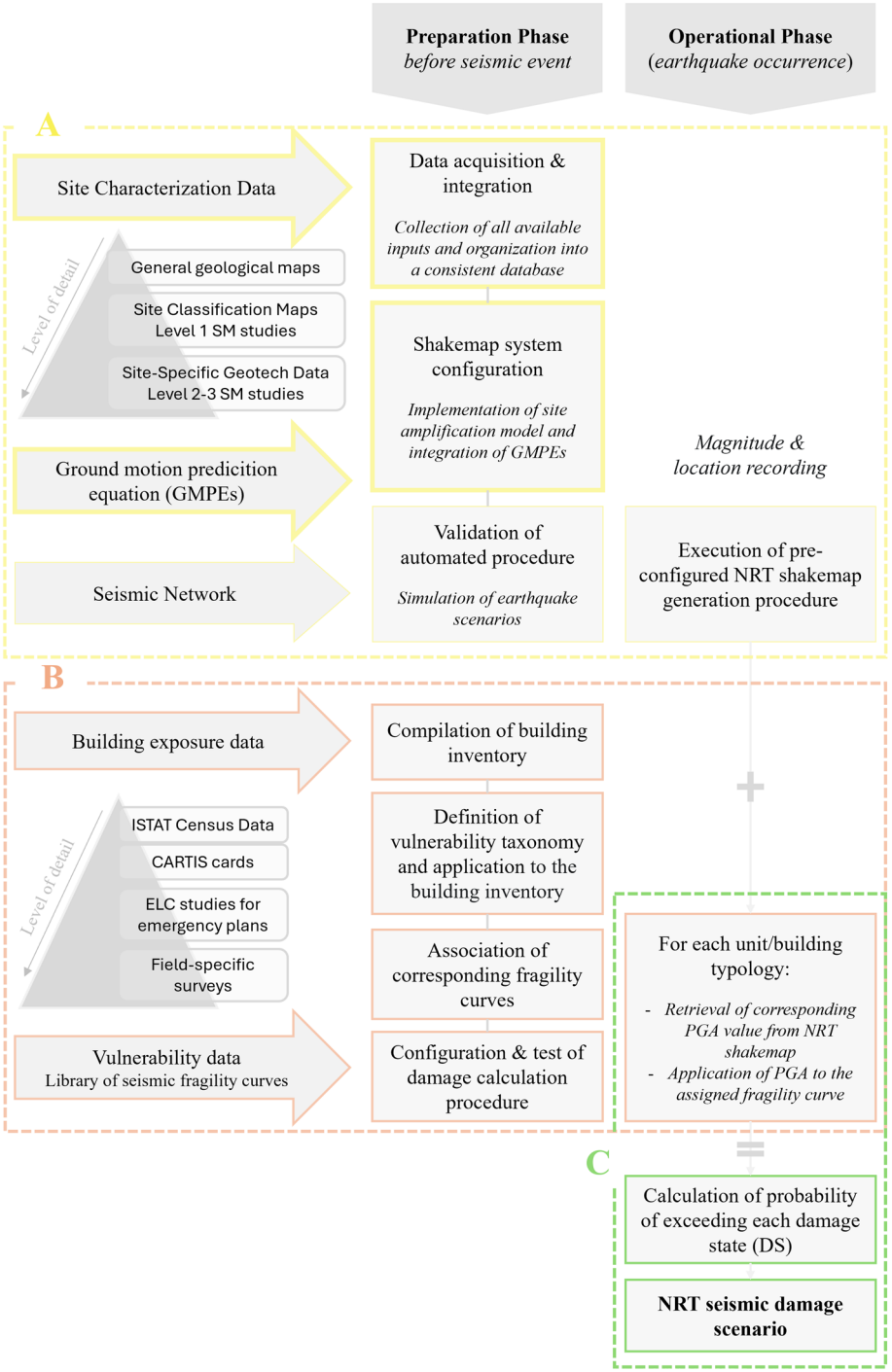

Fig. 1 Flowchart of the proposed methodology to generate near-real-time shakemaps and building damage scenarios for municipalities and urban centres

ing how different levels of information in the hazard and exposure affect the final damage results. The core process can be summarized in three main steps:

- Step A – Generating a Near-Real-Time (NRT) shakemap to quantify the seismic hazard input across the area of interest.
- Step B – Characterizing building exposure and vulnerability to assess the building stock's vulnerability by assigning specific fragility curves based on a detailed taxonomy, with a focus on residential buildings.
- Step C – Developing the seismic damage scenario by combining hazard (Step A) and vulnerability (Step B) to estimate the geographical distribution and severity of physical damage.

Following the earthquake, step A produces ground shaking maps (shakemaps in the following), which provide a georeferenced representation of key ground motion parameters, such as Peak Ground Acceleration (PGA), Peak Ground Velocity (PGV), and Spectral Acceleration corresponding to a given response period (Sa(T)), or seismic intensity (e.g., according to the modified Mercalli intensity scale). Generating NRT shakemaps requires an automated workflow that integrates several essential components. This workflow begins with seismic event information, which is typically provided by monitoring networks such as the Italian Seismic Network (Istituto Nazionale di Geofisica e Vulcanologia (INGV), 2005) and the Regional Seismic Network of Northwestern Italy (University of Genoa 1967) and includes earthquake location, magnitude, and origin time. Geological and geotechnical characterization is indispensable, as local subsurface conditions strongly influence the seismic shaking at the surface. This generally involves using soil classification maps to derive amplification factors. In this study, the procedure integrates detailed information from MS studies into a stand-alone procedure for shakemap generation. Ground Motion Prediction Equations (GMPEs) are employed to estimate the ground motion level on a reference site wherever instrumental recordings are not available. Finally, the procedure involves the integration of all this information: it amends the estimated rock-site shaking with local amplification factors, incorporates available instrumental recordings, and uses a spatial interpolation algorithm to generate a continuous shakemap across the study area. Procedure A in Fig. 1 is designed to perform these tasks sequentially and efficiently, delivering the NRT shakemaps as the core hazard input for the subsequent stages.

Step B focuses on establishing the building stock's vulnerability and exposure model. This step, which is independent of step A, consists of constructing the exposure model for the study area, associating each considered spatial unit (ideally a single building, often a census tract or another meaningful territorial unit) with a probabilistic or deterministic distribution of building typologies. The assessment of structural vulnerability primarily involves the use of seismic fragility curves, which can be derived through various approaches (da Porto et al., 2021). For urban scale assessment, it is crucial to select or develop specific fragility curves that are as representative as possible of the construction typologies in the study area and calibrated to local building practices and seismic design levels over time. To effectively employ fragility curves, it is necessary to classify the exposed building stock into homogeneous vulnerability classes using an appropriate taxonomy. The choice of an appropriate taxonomy requires a balance between the desired level of detail for an accurate vulnerability representation and the actual availability and quality of exposure data on an urban scale. In

Italy, a common building taxonomy uses attributes available from ISTAT CENSUS data for the entire national territory. For building stock, the ISTAT database provides basic information at the census tract level, including the predominant material (e.g., masonry, reinforced concrete, or others), construction period, and number of stories. However, the way this data is typically provided imposes significant limitations: information is aggregated at the census tract level (a territorial unit defined on a socio-economic basis), and crucially, the data for these attributes is reported independently, lacking cross-tabulation. Hence, to identify building typologies (i.e., characterized by unique combinations of these attributes) within any given census tract or to associate them with a single building implies the introduction of some aggregation rules.

Several highly detailed international taxonomies have also been proposed, such as those developed within the SYNER-G project (e.g., Lagomarsino and Cattari 2013; Pitilakis et al. 2014), the GEM (Global Earthquake Model) taxonomy (Brzev et al. 2013), those by initiatives like GED4ALL (e.g., Silva et al. 2018), which focused on standardizing detailed attributes for global exposure databases, and the GLOSI (Global Library of School Infrastructure) taxonomy (Adhikari et al. 2023), which was specifically developed for school buildings.

In the present application, the characterization of the masonry building stock was defined based on the SYNER-G taxonomy with the aim of integrating predominant material and number of stories with other structural details, such as diaphragm or masonry types. In general, the complete application of detailed taxonomies is rarely feasible for extensive inventories covering entire cities, due to the difficulty in gathering all necessary information for each building. To partially overcome these limitations and achieve a more refined characterization of exposure on the urban scale, the methodology proposed here (Procedure B) integrates, when available, data from more refined sources. Among these, data derived from the CARTIS project (Zuccaro et al. 2023) provides valuable statistical information on specific building sub-typologies. The CARTIS studies involve a systematic methodology for collecting data on ordinary buildings, which are grouped into "sectors" (areas that are homogeneous in terms of construction type and age). Data collected for the built environment encompasses the number of storeys, the age of construction, types of masonry, various floor slab types, the presence or absence of connecting elements such as tie rods, and other important structural information. The objective is to enhance seismic vulnerability data and risk estimates at both the municipal and sub-municipal level (Polese et al. 2019). This data can be used to disaggregate the aggregated ISTAT classes in a more informed manner or to guide a more accurate selection of representative fragility curves for each area. Another relevant source is the ELC analysis. The ELC, which is detailed in operational guidelines and evaluation methodologies developed by IDPC (e.g., Dolce 2012), aims to evaluate the effectiveness of the municipal emergency plan in the event of an earthquake (Dolce et al. 2018). These analyses provide point or area-specific information on critical elements of the urban system (e.g., strategic buildings such as town halls, hospitals, schools, fire/police stations, essential infrastructures such as roads and bridges, or buildings whose collapse could obstruct access routes). Integrating ELC data allows for a targeted vulnerability assessment of strategic components of the city, particularly critical for emergency management.

Once the hazard input from Step A and the exposure/vulnerability model from Step B are established, Step C estimates the damage scenario. The selection of the specific Intensity Measure (IM) (Kohrangi et al. 2016) driving this analysis is crucial and often guided

by practical considerations, primarily the format of available fragility functions. Although spectral acceleration at relevant periods might offer higher accuracy in predicting damage for specific structures, many existing fragility curves, especially those developed for regional or national scale assessments, are formulated based on PGA. Consequently, PGA is adopted here as the primary IM to maximize compatibility with readily available and widely used vulnerability models. For each building, our procedure first retrieves the relevant PGA value from the NRT shakemap corresponding to its location. Then PGA is used with fragility curves and building counts to estimate expected damage levels at census tracts and generate thematic maps depicting the expected damage distribution across the entire urban area or census tracts, as well as the percentage of unsafe and collapsed buildings or other losses by introducing appropriate consequence functions.

Finally, as illustrated in Fig. 1, this methodology is applied in two distinct temporal phases:

- **Preparatory stage** (before the seismic event occurrence): this is a crucial, time-consuming, and resource-intensive phase. It encompasses the collection, organization, homogenization, and system implementation of all necessary information. This includes collection of geological and geotechnical data for site characterization, the definition of an up-to-date building inventory (drawing from CENSUS, CARTIS, ELC, ad-hoc surveys), the critical selection or development and implementation of suitable fragility curves, and the configuration and thorough testing of the automated procedures for shakemap generation (Step A) and damage estimation (Steps B and C).
- **Operational phase** (upon event occurrence): this phase, activated upon the detection of a potentially damaging seismic event, involves the system executing the pre-configured procedures corresponding to Steps A, B, and C in sequence. This phase must be rapid –ideally operating in minutes– to generate the NRT damage scenario swiftly enough to be useful for guiding initial and critical emergency management actions.

In the context of the present study, the general framework illustrated in Fig. 1 is applied to the municipality of Sanremo (Sect. 3) to specifically investigate the influence of input data detail on the resulting damage scenarios. While the workflow encompasses the complete chain from hazard to damage assessment, this paper focuses on a multi-level comparative analysis, contrasting scenarios derived from standard national-scale data with those enriched by detailed site-specific information. It is worth noting that the proposed architecture is designed to be modular and scalable; therefore, while this specific application adopts deterministic choices for certain parameters to test the sensitivity of the results, the framework paves the way for future developments–such as the integration of real-time monitoring networks and the systematic quantification of epistemic uncertainties–which are further discussed in the concluding remarks.

3 Overview of the pilot study area: the municipality of Sanremo (IM), Italy

The municipality of Sanremo was chosen as a case study because it offers numerous pre-existing studies, including CARTIS analyses, ELC studies, and an accurate seismic microzonation research conducted by the University of Genoa in collaboration with the Sanremo municipality and the Liguria Region. Additionally, ad-hoc on-site surveys were performed on a selected area of the city of Sanremo to gather more detailed information on building characteristics, such as structural type, number of stories, and significant structural details or geometric irregularities in plan and elevation, with a building-by-building granularity (significantly more detailed than that provided by ISTAT CENSUS data).

3.1 Structural characterization of the existing built environment

Sanremo has a remarkably interesting building heritage, subdivided into different historical phases and marked by a variety of construction types and materials, mirroring the economic, cultural, and urban evolution of the city. A detailed characterization of the existing buildings highlights the specificities associated with each construction period, including structural vulnerabilities, material choices, and construction techniques, with particular emphasis on seismic safety issues and material degradation – aspects which were investigated in detail within the context of studies on the Ligurian historic centres, including Sanremo (Chirico et al. 1992). According to this study, Sanremo's buildings can be grouped into four primary historical periods (Fig. 2). Like many coastal towns in Liguria, the city originated as a fortified settlement with architecture primarily designed for defence. The historic district "La Pigna" (Fig. 2a) represents the medieval core, characterized by irregular streets and massive

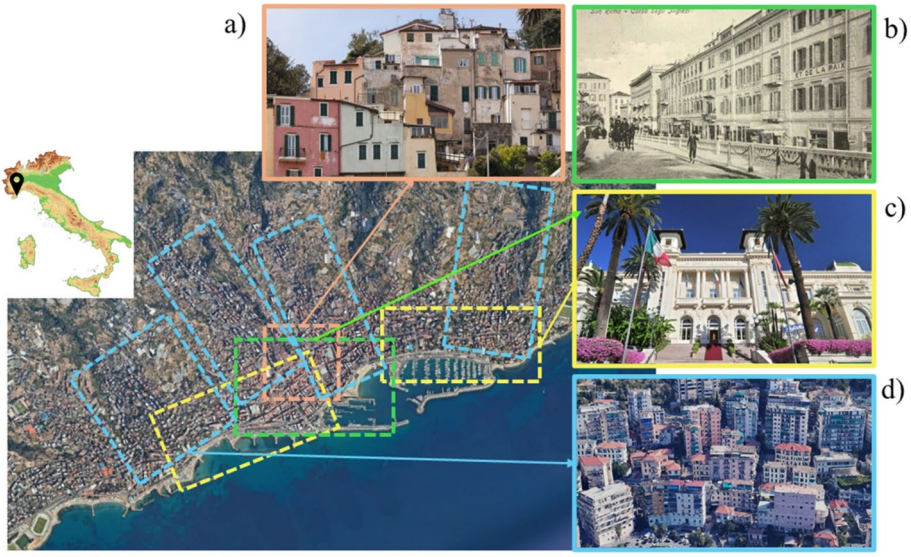

Fig. 2 Sanremo's buildings can be classified into four historical periods: (**a**) the medieval "La Pigna" district, (**b**) 19th-century classical-style residences, (**c**) late 19th–early 20th-century Art Nouveau architecture, exemplified by the Casino, and (**d**) post-war expansion with reinforced concrete structures

limestone masonry buildings, typically three to four stories high, with weak mortar and wooden pitched roofs. In the 19th century, the city expanded beyond the medieval centre, with new residential buildings and palaces in a classical style (Fig. 2b). These masonry structures feature thinner walls, metal beams for reinforcement, and wooden or steel floors, but lack effective seismic connections. By the late 19th and early 20th centuries, Sanremo embraced the *Art Nouveau* architecture, incorporating reinforced concrete and steel elements. Iconic buildings such as the Casino (Fig. 2c) showcase elaborate decorations, but balconies and cornices, often made of wrought iron, are prone to corrosion. Post-World War II, the city expanded into suburban areas with modern residential districts. Reinforced concrete and steel allowed for taller, standardized buildings – typically five to six stories – with simpler, more functional designs compared to earlier elaborate styles (Fig. 2d).

Using information available from the ISTAT database for each census tract of the Municipality of Sanremo, we developed exposure maps (Fig. 3) in QGIS software (version 3.34.9-Prizren). In particular, Fig. 3a shows the built density within the census tracts, highlighting that residential buildings are primarily concentrated in the historic centre (roughly corresponding to the light-orange square in Fig. 2) and along the coast. The predominant construction type (Fig. 3b) is unreinforced masonry (URM), followed by reinforced concrete (RC) in expansion areas, while other materials (mixed masonry and RC structures, wood, steel, etc.) appear only in a few sections. The construction period (Fig. 3c) varies significantly: buildings from the pre-1919 class are primarily located in the historic centre, whereas in sections where reinforced concrete is predominant, the buildings typically date to the post-war period. Finally, Fig. 3d shows the distribution of buildings based on the

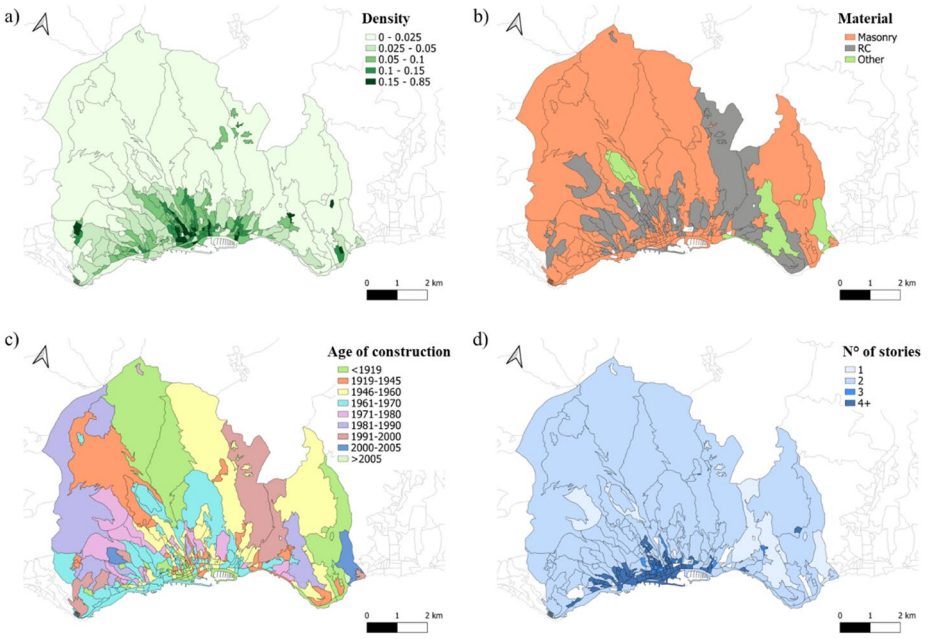

Fig. 3 Representation of exposure at the census tract scale based on (**a**) residential built density, (**b**) predominant construction type, (**c**) predominant construction period, and (**d**) predominant number of storeys

number of floors: two-storey buildings are prevalent; however, in the most densely built areas, the predominant number of storeys is four or more.

To gather detailed information on Sanremo's built environment, on-site surveys were conducted in a selected area of the city, including the city center, the Pigna district, the waterfront, and some important streets. Notably, this area is also crucial for the ELC system and critical for the recovery phase, as emerged in Cattari et al. (2024) through a study that directly involved the local administration. During the survey campaigns, which involved more than one thousand buildings, we collected data on building material (using a thermal imaging camera, Fig. 4), number of floors, presence of structural details such as tie rods and RC edge beams, regularity in plan and elevation, and their configuration (isolated or in aggregate). Figure 5 shows the resulting exposure maps developed in the QGIS environment, illustrating the distribution of buildings based on building material (Fig. 5a) and number of storeys (Fig. 5b). Moreover, the period of construction (Fig. 5c) has been derived from ELC data and previous studies regarding the evolution of the built environment throughout various epochs. Finally, Fig. 5d depicts the resulting "ISTAT" sub-typologies, defined by the combination of material and number of storeys. Most buildings are made of masonry (approximately 77%) and have four or more floors (around 59%). More specifically, as shown in Fig. 5d, most URM buildings located in the older, more consolidated urban areas also have four or more floors. RC buildings, which are mainly located in the post-war urban expansion zones, also typically have more than four storeys. Overall, the predominant construction period is pre-1919.

3.2 Characterization of local seismic hazard

Sanremo is located in a region of moderate seismic activity, with a documented history of damaging earthquakes. Notably, the destructive 1887 Ligurian Sea earthquake, with an estimated magnitude of 6.3, significantly affected the city and surrounding areas, causing

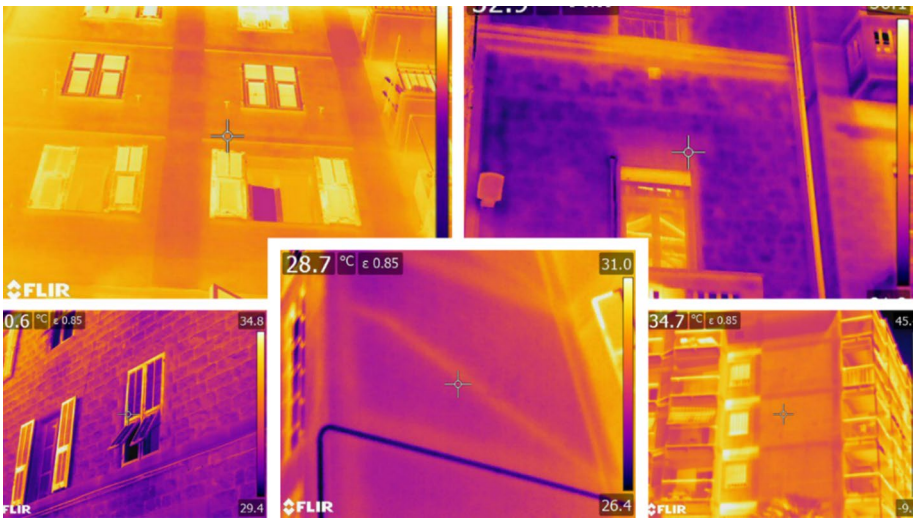

Fig. 4 A selection of thermographic images captured during on-site surveys illustrating different materials (masonry and reinforced concrete) and construction types in the examined buildings

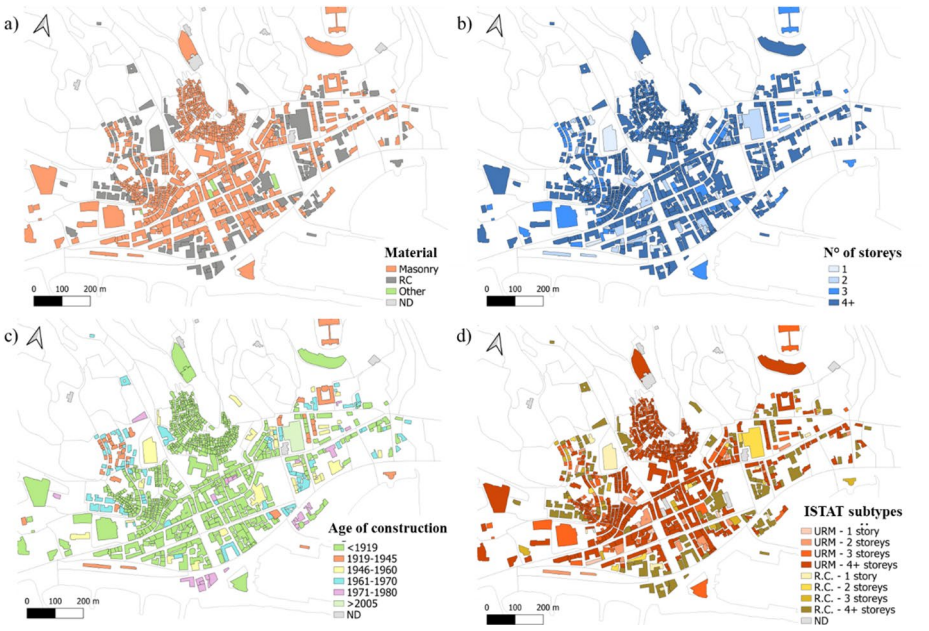

Fig. 5 Maps illustrating, for a selected area of Sanremo, the distribution of buildings based on (**a**) building material, (**b**) number of storeys, (**c**) age of construction, and (**d**) combination of material and number of storeys

considerable damage and highlighting the vulnerability of the building stock. While the 1887 event remains the most significant historical earthquake, other moderate-to-strong events have occurred in modern history: the 1818 and 1831 western Liguria earthquakes with moment magnitude (M_w) equal to 5.3, 5.6, and 5.7, respectively (Rovida et al. 2022). More recently, ground shaking induced by earthquakes in the nearby Alps-Maritimes border region (France/Italy) was occasionally felt in Sanremo, along with smaller, more localized offshore or inland seismic sequences within the Liguria region. This seismic background highlights the need for a rigorous assessment of local seismic hazard that accounts for specific site conditions (e.g., Barani et al. 2020), a fundamental step for estimating seismic risk within the municipality. This characterization aims to understand and quantify site effects, including amplification phenomena that are influenced by local, near-surface geological and geotechnical conditions. Within the scope of the present study, a systematic comparison was conducted between the different amplification factors estimated for the Municipality of Sanremo, evaluated specifically at the centroids of each building surveyed in the study area (as described in detail in Sect. 3.1).

Seismic microzonation (MS) studies are crucial to achieve this goal. These studies can be conducted at increasing levels of detail. While first-level MS studies map stable areas, stable areas susceptible to amplification, and unstable areas potentially prone to secondary hazards such as landslides or liquefaction, higher-level MS studies provide a quantification of such earthquake-induced effects through simplified approaches (second level) or numerical simulations (third level). For the Municipality of Sanremo, third-level MS studies results are available from the government of the Liguria Region. Specifically, they quantify local

ground motion amplification through Amplification Factors (FA) defined across different frequency (period) ranges that reflect structural response (i.e., 0.1–0.5 s, 0.4–0.8 s, and 0.7–1.1 s).

The availability of MS studies, however, is not uniform across all municipalities nationwide. Consequently, amplification effects are often quantified through simplified approaches based on simple geotechnical and geological parameters. Commonly, building codes and GMPEs use site correction terms that quantify the level of amplification as a function of the well-known $V_{s,30}$ parameter, defined as the time-averaged shear wave velocity in the upper 30 m of soil. Similarly, the Italian building code classifies soils as a function of the value of the equivalent shear wave velocity above the bedrock (defined as the formation with V_s not less than 800 m/s), $V_{s,eq}$. Applying these latter approaches over large areas requires the availability of maps showing the spatial distribution of these key parameters. In the present study, the $V_{s,30}$ values for each building centroid were derived by interpolating values from the national-scale grids provided by Mori et al. (2020) or Forte et al. (2019). These studies represent an important step in this direction, as they propose $V_{s,30}$ and/or $V_{s,eq}$ maps for all of Italy based on geological and geomorphological data as well as on site-specific geotechnical and geophysical measurements (especially from seismic microzonation studies).

Figure 6 shows the results of this comparison for the PGA scenario of the 1887 Western Liguria earthquake with magnitude 6.3. According to Barani et al. (2007), we assumed an offshore epicenter with longitude 8.13° E, latitude 43.74° N. Specifically, Fig. 6a shows the earthquake epicenter and, for each examined building centroid, the corresponding PGA value on rock. Figure 6b shows the spatial distribution of the different amplification factors described above for Sanremo. These include: the FA factor obtained from third-level MS studies, the site term (F_S) from the most recent Italian GMPE of Lanzano et al. (2019) (hereinafter, referred to as ITA18), which we use as a reference in the present research, and the stratigraphic coefficient (SS) calculated using the NTC18 formulation. While F_S is a linear amplification term based on $V_{s,30}$ (to derive the values of $V_{s,30}$, we use separately the maps of Forte et al. (2019) and Mori et al. (2020), SS takes into account soil non-linearity through the $V_{s,eq}$ parameter, whose values were determined from the Forte et al. (2019) map. To effectively apply the amplification factors (FA) derived from the aforementioned MS studies, which are defined for specific period bands, we first had to determine the fundamental vibration period (T_1) for each building. It was calculated as a function of its height (H) and a coefficient (C) that primarily depends on the structural type and building material, according to the simplified formula $T_1 = C \cdot H^{3/4}$ proposed in the Italian building code NTC18 (Ministero delle Infrastrutture e dei Trasporti 2018). Although the mathematical formulation of these amplification factors is fundamentally different, we note the following: the $V_{s,30}$ values derived from the Mori et al. (2020) map, which shows a finer spatial resolution compared to those from the Forte et al. (2019) map, tend to produce slightly higher amplification factors. However, a crucial observation is that both these national-scale approaches tend to yield average amplification factors lower than those derived from the third-level MS. This discrepancy underscores the intrinsic value of in-depth local investigations in capturing the local seismic response details, which national-scale models may miss.

To illustrate how these methodological differences translate into different estimates of seismic input (in terms of PGA) at the scale of individual buildings, Fig. 6c presents a comparison for two sample buildings selected within the study area. In particular, the figure illustrates the amplification factors calculated using the various approaches discussed previ-

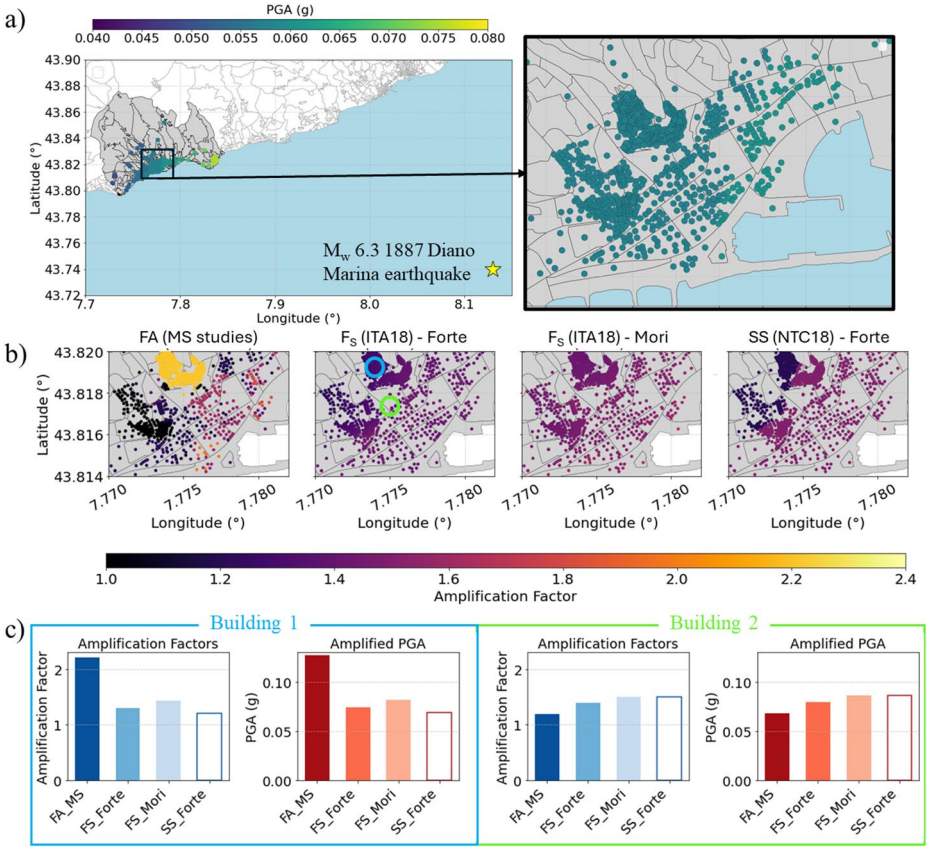

Fig. 6 (**a**) PGA scenario of the 1887 Western Liguria earthquake with magnitude 6.3 and an offshore epicenter of longitude 8.13° E, latitude 43.74° N (Barani et al. 2007), (**b**) comparison of different amplification factors for the centroids of the buildings in the study area and (**c**) site amplification factors and corresponding amplified PGA values for two example buildings, where the green dot is for building 1 and the blue dot is for building 2. The "Forte" or "Mori" designation indicates that $V_{s,30}$ values for F_S calculation are taken from either Forte's or Mori's map, while $V_{s,eq}$ values to calculate SS factor are from Forte's map

ously, as well as the resulting impact of these factors on the ground shaking level. The site-specific PGA values are obtained by multiplying each amplification factor by the rock PGA calculated for the 1887 Western Liguria earthquake (Fig. 6a). Figure 6c highlights how the choice of the amplification factor can lead to significantly different estimates of the seismic demand for the same location and seismic event.

4 Elaboration of seismic damage scenarios

4.1 Generation of near-real-time maps of ground motion

As previously mentioned, NRT ground shaking maps are typically produced by combining real ground-motion recordings with predictions from a GMPE. Alternatively, predictions from empirical ground motions can be replaced by ground motions computed through stochastic approaches and/or numerical simulations that account for fault rupturing and seismic wave propagation. Regardless of the approach used to estimate the surface ground-shaking (i.e., empirical, stochastic, or synthetic), amplification effects should be considered to avoid underestimating the shaking level.

In the present study, we developed a stand-alone procedure that couples real ground motions from monitoring stations with empirical ground-shaking values. This utility has the following key features:

1. Compatibility with seismological standards and interoperability with common procedures used by seismological networks (e.g., procedures aimed at earthquake detection, determination of earthquake location and magnitude). To achieve this, the utility was developed considering the monitoring procedures currently in use by the Regional Seismic Network of Northwestern Italy (University of Genoa 1967).
2. Use of up-to-date GMPEs to compute scenarios in areas that monitoring stations do not cover.
3. Implementation of geological data from different sources (e.g., outcomes from seismic microzonation studies) to account for site-specific amplification effects.

To speed up computation time and increase flexibility, the estimation of ground-motion values via the GMPE at hand was decoupled from the overall procedure and treated as an independent step. Specifically, the selected GMPE, the ITA 18 model proposed by Lanzano et al. (2019) for shallow crustal earthquakes in Italy, is used to generate a database of ground-shaking values on rock for different magnitude-distance pairs. The database is then queried (via an algorithm in Python) using the values of magnitude and source-to-site-distance determined following the earthquake, and the corresponding ground-motion values on rock are adjusted using an additional term to account for local soil conditions. This allows for maximum flexibility in incorporating amplification effects, which can be determined from specific microzonation studies or defined as a function of the well-known $V_{S,30}$ parameter (details on the amplification factors considered in the present study can be found in Sect. 3.2). The code can generate ground-motion scenarios in terms of peak ground acceleration (PGA) and spectral acceleration for different response periods ($S_a\,(T)$), and handle the variability associated with the ground motion.

In addition, intensity scenarios (using the Mercalli-Cancani-Sieberg scale) can be produced by converting PGA values into intensity levels using empirical relationships (the utility currently implements the models developed by Faenza and Michelini (2010) and Oliveti et al. (2022).

4.2 Adopted seismic fragility models for residential buildings

In this paper, we adopt the well-established lognormal model for fragility curves, which defines the conditional probability $P_{DS|IM}$ that a given Damage State (DS) is exceeded for a given value (im) of an Intensity Measure (IM) of the seismic event:

$$P_{DS|IM} = \Phi\left[\frac{\ln im - \mu_{\ln IM,DS}}{\beta_{DS}}\right], \tag{1}$$

where Φ is the standard normal Cumulative Distribution Function (CDF), $\mu_{\ln IM}$ is the mean logarithmic *IM of the given DS*, and $\beta = \sigma_{\ln IM}$ is the dispersion of the *IM for the same DS* (Lagomarsino and Cattari, 2013). In this paper, four DSs are considered (DS1: Slight Damage, DS2: Moderate Damage, DS3: Extensive Damage, and DS4: Partial Collapse), which are conceptually consistent with the EMS-98 scale. Using this model, fragility functions are defined by two parameters: the median intensity IM (i.e., $\mu_{\ln IM,DS}$) and the associated variability (β_{DS}), aimed to incorporate the impact of various uncertainty sources (e.g., on the seismic input, the structural response, the definition of DS).

As previously mentioned, the selection of fragility curves should be based on appropriate criteria, ensuring that they accurately represent the behavior of the structural system being examined. Several types of curves, developed through different approaches (i.e., empirical, numerical-mechanical and analytical-mechanical, and hybrid), are available in the literature. The works of Chieffo et al. (2019), Cattari et al. (2024), and da Porto et al. (2021) propose interesting comparative studies in which different approaches are benchmarked and tested. In this research, we adopted two different approaches. The first is the heuristic-macroseismic approach originally proposed by Lagomarsino and Giovinazzi (2006) and then refined in Lagomarsino et al. (2021). This method is called "heuristic" because it relies on assumptions derived from expert judgment, and "macroseismic" because it implicitly leverages the established framework of building vulnerability and expected damage at different macroseismic intensity levels (I) as defined by the European Macroseismic Scale EMS-98 (Grunthal et al., 1998). In the work of Lagomarsino et al. (2021), the approach has been generalized to represent the behavior of building typologies with different ductility/fragility by introducing a second free parameter, the ductility index Q, in addition to the vulnerability index V. The calibration of these parameters was supported by damage data from residential masonry and reinforced concrete buildings from the Da.D.O. (Database of Observed Damage) platform (Dolce et al., 2019), particularly for the 2009 L'Aquila and 1980 Irpinia earthquakes. Moreover, in Lagomarsino et al. (2021), for different ISTAT typologies (i.e., defined in terms of a combination of age of construction, material type, and number of stories), vulnerability curves are converted into fragility curves by assuming a proper I-PGA correlation law. In its original formulation, Lagomarsino and Giovinazzi (2006) introduced also some vulnerability modifiers to account for additional building characteristics, such as masonry typology, state of maintenance, quality of materials, planimetric regularity, regularity in elevation, interaction with adjacent buildings (aggregate), retrofitting interventions, and site morphology. However, an updated calibration of these modifiers has not been yet made available.

The second is the Displacement-Based Vulnerability (DBV) Masonry method (Lagomarsino and Cattari 2013), a mechanical-analytical approach developed for masonry build-

ings that yields a capacity curve representing the global in-plane seismic behavior of the structure, eventually adjusted on the displacement capacity through corrective factors to account also for the out-of-plane response. This curve is defined by three fundamental variables (the pseudo-elastic period T_y, the spectral acceleration at yield A_y, and the ultimate displacement d_u) that are evaluated using a limited set of mechanical/geometric parameters, an assumed fundamental modal shape, and correction factors (K_i) that account for construction details and morphological characteristics. The method explicitly assumes – through a mechanical formulation –a diagonal shear failure in piers (Strong Spandrel Weak Piers - SSWP, weak story), but the other damage modes (Weak Spandrels Strong Piers - WSSP, or intermediate behaviour accounting for the flexural damage mode too) are likely to be simulated through the aforementioned correction factors. Subsequently, a nonlinear static procedure uses over-damped spectra (Freeman, S. A., 1998) to calculate the median IM required to reach specific damage levels. The derivation of fragility curves is finally funded on the adoption of the surface response technique to explicitly propagate uncertainties arising from the seismic demand and the structure's capacity.

In the paper, the two methodological approaches were compared based only on their resulting fragility curves, since the different hypotheses and parameters behind them made a comparison of intermediate steps impractical.

4.3 Downscaling process for exposure data and vulnerability models

4.3.1 Taxonomy and fragility curves at national and urban scale

As introduced in Sect. 2, the building's exposure is herein characterized in terms of ISTAT data or information acquired from in-situ surveys. In both cases, the association of the fragility curves to the building stock implies the attribution of three main parameters: age of construction, number of stories, and material (i.e., URM or RC). However, the fragility models may be informed by a more detailed list of attributes. Compared to more standardized and engineered structures (e.g., RC buildings), masonry buildings, which frequently represents a non-engineered construction type, display greater intrinsic variability in materials, construction techniques, and structural details. Consequently, the seismic performance of masonry buildings is highly sensitive to local building practices and historical evolution, making them especially susceptible to regional variations and territorial specificities. In particular, to downscale vulnerability data from the national to the urban scale, we characterize the masonry building stock using the SYNER-G taxonomy (Lagomarsino and Cattari 2013), focusing particularly on a subset of its attributes: Force Resisting Mechanism Material (FRMM), Details and Maintenance (DM), Floor System (FS), and Height Level (HL). For a more comprehensive description of the SYNER-G taxonomy, the reader may refer to Table A1 reported in the Annex of this paper. Within the framework of the SYNER-G taxonomy, the construction period served as a proxy to define the DM and FS attributes, leveraging statistical information provided for the Sanremo case by studies derived from the CARTIS project. The FRMM attribute categorizes the masonry type based on its material and construction technique. In the present study, data from CARTIS wall typologies are converted into masonry typologies in line with those proposed in the Italian building code (NTC18), which provides reference mechanical parameters used to define the mechanical models. The FS differentiates among rigid, flexible, and vaults diaphragms. The DM

attribute, on the other hand, describes the presence and quality of constructive details that enhance seismic performance, such as tie rods or ring beams (associated with the "High Quality" condition). The CARTIS data originally groups these two structural details (since both are assumed useful to prevent or at least reduce the activation of out-of-plane mechanisms), thus preventing any distinction of recurrent specificity between the two. However, since the DBV-masonry model differentiates the corrective factors as a function of these two aseismic devices, the distinction between tie rods and ring beams was driven by the construction age. When the prevalent construction era in the sectors is "<1919", the presence of ring beams is not hypothesized; consequently, whenever in CARTIS forms "High Quality" is identified, it refers specifically to tie rods. For the sectors present in Sanremo, given the prevalent construction era (from CARTIS data) and the indicated floor typologies (which belong to the family of flexible floors and vaults), the most plausible hypothesis is that the percentage corresponding to "ring beams or tie rods" actually represents tie rods.

The CARTIS data enriches information from ISTAT or rapid on-site surveys, specifically for masonry typologies and constructive details, but it does not replace them. For aspects like material, number of floors, and age of construction, the CARTIS data is less comprehensive since the CARTIS form provides information only on dominant classes, but it is not exhaustive in covering all building stock. Figure A1 in the Annex shows the division of Sanremo into sectors and provides a summary of information for those areas dominated by masonry buildings. Based on the data collected for each sector (summarized in Table A2 in the Annex), Sanremo's building stock is primarily characterized by 2 specific FRMM types, 2 DM classes, 3 FS types, and 4 HL categories (Table A3 in the Annex).

As far as the fragility curves are concerned, hereafter, we refer to two different scales such a *national* and *urban*. The designation *national-* clarifies that the approaches introduced in Sect. 4.2 are used through fragility curves developed for building typologies representative of the national stock, commonly used in large-risk assessment studies. Instead, with the *urban-* label we refer to the model informed by CARTIS data and, consequently, to the more refined attributes selected from the SYNER-G taxonomy. The *urban-* format is thus the one specifically calibrated using the detailed characteristics of the Sanremo building stock, (i.e., "sector-specific"). For this study, the DBV-*Masonry* model was selected for the detailed urban assessment due to its flexibility and capability of quantifying the impact of different material properties and structural details through a mechanical approach. Even though the alternative heuristic model was recently updated (Lagomarsino et al. 2021), with its fundamental parameters (V and Q) recalibrated on observed damage data, a coherent set of vulnerability modifiers consistent with this new calibration is not yet available. Furthermore, the DBV-Masonry model is inherently better suited for this detailed application as it directly captures the characteristics of the building stock through its mechanics-based parameters, rather than relying on modifiers defined for broad macro-typologies.

Among the mechanical and geometrical parameters on which the DBV-masonry model is based, some of them are directly linked to the attributes FRMM, FS, and DM. In particular, the model considers 10 FRMM typologies, 4 FS types, and 3 DM categories. The possible combinations of these alternatives lead to a set of 120 fragility curves for each number of stories, shown in light grey in Fig. 7a for the DS3 Damage State. These curves are then grouped according to a logic tree approach, assigning appropriate weight to each branch (i.e., resulting from a combination of FRMM/FS/DM realizations). In the case of *national-* format, these weights have been attributed starting from the data of Da.D.O. platform for the

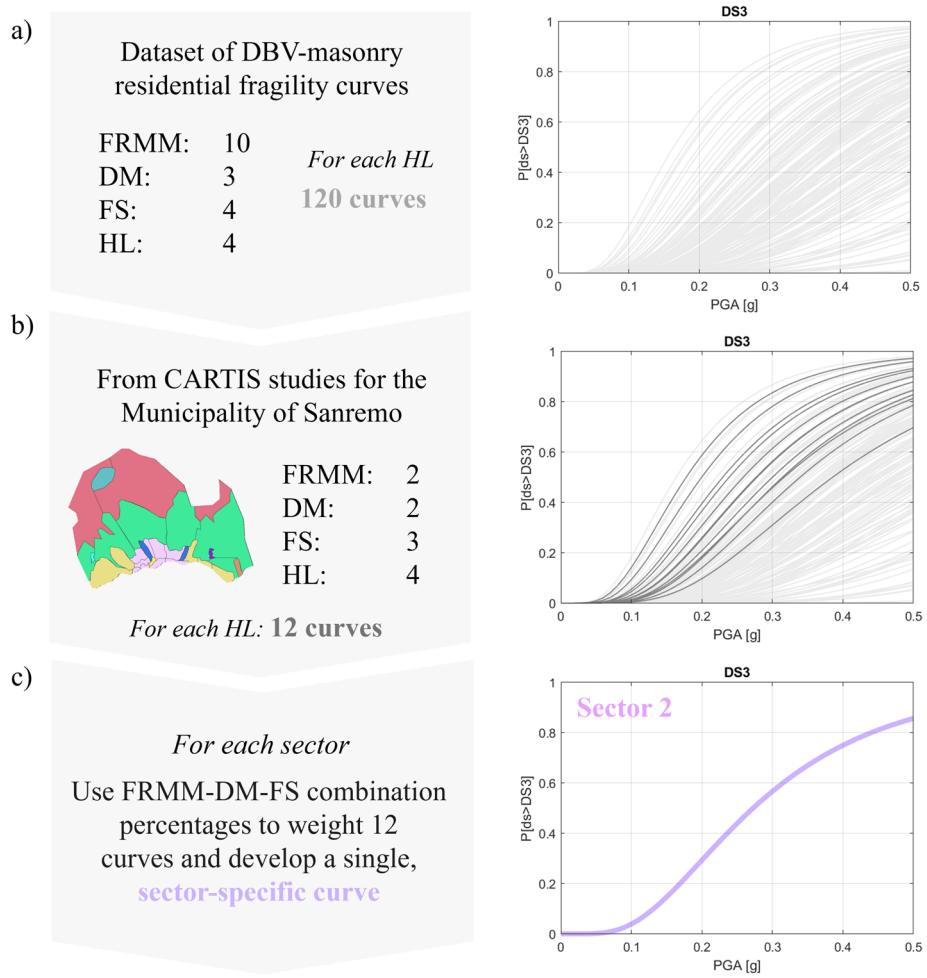

Fig. 7 Derivation of sector-specific fragility curves for the case study of Sanremo. (**a**) 120 initial DBV-masonry curves (per each height level class), (**b**) selection of 12 curves for an example sector (Sector 2), (**c**) final weighted curve using combination percentages reported in Table A4 in the Annex

L'Aquila 2009 earthquake and slightly adjusted to be representative of the overall Central Italy. In the case of *urban*- format, conversely, only the branches associated with the actual combination representative of the Sanremo municipality and resulting from the CARTIS study were considered, leading to a subset of 12 fragility curves for each number of stories.

For the DS3 damage state, the 12 curves are shown in dark grey in Fig. 7b. Given the percentage of each specific FRMM-DM-FS combination within a specific sector (data provided in Table A4 of the Annex), these curves can be weighted to yield a single fragility curve representative of the average vulnerability of that specific sector for a given HL and DS (shown in Fig. 7c for sector 2 and DS3).

Figure 8 compares the *national* heuristic model (light blue curve) and the *national* DBV-Masonry model (pink curve) for URM buildings, and the *national* heuristic model (black

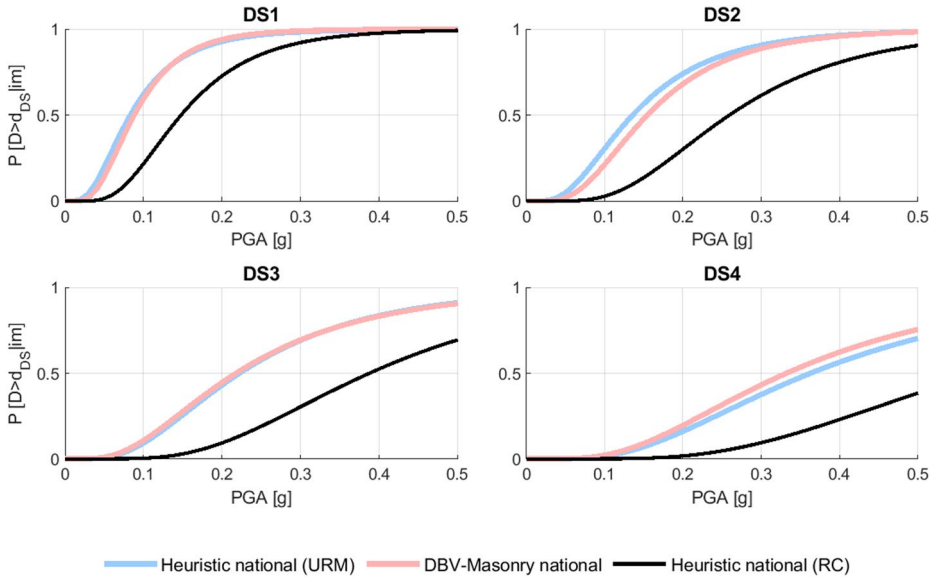

Fig. 8 Comparison between the fragility curves from the national heuristic model and the national analytical-mechanical DBV-model for unreinforced masonry (URM) structures and the national heuristic model for reinforced concrete (RC), where DS1: Slight Damage, DS2: Moderate Damage, DS3: Extensive Damage, and DS4: Partial Collapse

curve) for RC. For RC structures, the curve adopted is for buildings designed exclusively for gravity loads: this reflects the assumption that the vast majority of Sanremo's RC building stock was constructed before the implementation of comprehensive seismic design codes following the 2003 national seismic classification (OPCM 3274/2003).

Finally, to highlight how sector-specific curves calibrated with CARTIS data can deviate from the national model, Fig. 9 presents a more focused comparison. For the <1919 construction period, DL2 and DL3 damage states, and three storey classes (2-storey, 3-storey, and higher than 4-storey), the figure compares the national DBV-Masonry model curve (black curve) with the specific fragility curves for Sanremo sectors within that sub-typology, which were defined using the DBV-Masonry method and CARTIS data (coloured curves) and derived using the approach illustrated in Fig. 7c. This comparison reveals a noticeable variation in the estimated fragility, highlighting how sensitive the results are to the specific characteristics of the building stock under analysis. Of course, this result is not general and depends on how the specific features of the examined building stock deviate from the national reference.

4.3.2 Disaggregation of ISTAT census data to estimate building sub-typologies

For each census tract, ISTAT provides key information on the building stock, specifically the total number of buildings for each material type (masonry, reinforced concrete, or other), for each construction period (<1919, 1919-45, 1946-60, 1961-70, 1971-80, 1981-90, 1991–2000, 2001-05, >2005), and for each storey class (1, 2, 3, or >4). The treatment of these storey classes, especially the ">4" category, is particularly critical for vulnerability assess-

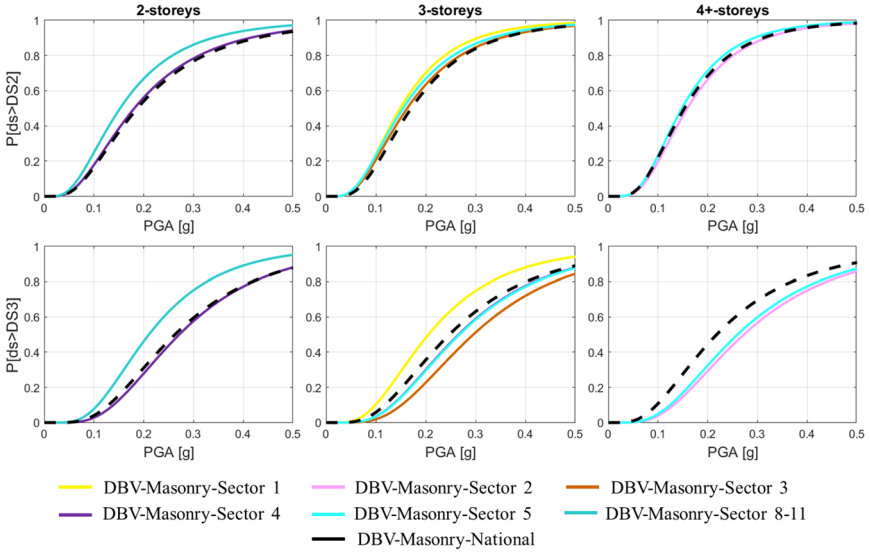

Fig. 9 Comparison between the fragility curves obtained by applying the national DBV model and the DBV method (informed by data from the Sanremo CARTIS sheets)

ments (e.g., Lagomarsino et al. 2021), and is a key aspect addressed by national initiatives, such as the MARS project for school buildings, which specifically uses the ISTAT 2011 classification for its fragility curves (Lagomarsino and Masi 2022). However, this data is provided as separate, aggregated totals for the entire census area, making it impossible to link these attributes on a building-by-building basis. The total counts for the section are known, but not the attributes or location of any single structure. For example, while the number of masonry buildings in each census tract is provided, the data does not specify how many of them were built before 1919, or how many have two stories. The primary objective of the procedure detailed here is to disaggregate this census data to estimate the number of buildings for each specific sub-typology, which is defined by the combination of these three taxonomic parameters (e.g., estimating how many masonry buildings built before 1919 have two stories).

To achieve this, we implemented a rule-based, sequential disaggregation procedure to distribute the aggregated census data among each sub-typology, implemented through a Python algorithm. First, the algorithm classifies buildings according to material and age of construction by following this sequence of rules:

1. The first step of the procedure assigns a construction period to the masonry buildings. The process begins with a key assumption: all buildings from the earliest construction period (< 1919) are made of masonry. If the total number of masonry buildings reported by ISTAT for a census tract exceeds the total number of buildings in this oldest period, the surplus masonry buildings are assigned to later periods. This is repeated sequentially, following the chronological order of the periods: 1919–1945, then 1946–1960, and so on. The algorithm fills each epoch with the remaining masonry buildings subject to two conditions: the number of masonry buildings must not exceed the total number

of buildings available in that epoch, and the procedure stops once all masonry buildings have been assigned. The process only moves to the next epoch after the current one has been filled or all masonry buildings have been assigned.

2. Buildings made with materials other than masonry and concrete (including steel, wood, and mixed-material structures) are processed next. These are preferentially assigned to a transition epoch, defined to range between 1919 and 1970. This epoch reflects the historical period in which the use of masonry was gradually substituted by reinforced concrete, with various possible hybrid structural solutions. Buildings identified by ISTAT as "other material" are gradually assigned to the remaining epochs following the procedure described at step 1, starting with the periods where the assignment of masonry buildings is complete.
3. Finally, RC buildings are assigned by difference. These fill all the remaining unassigned construction periods after "masonry" and "other material" buildings have been assigned. As a result, RC buildings are generally allocated to the more recent periods (e.g., after 1960).

After the disaggregation by material and age of construction is completed, the algorithm assigns the corresponding number of buildings to each storey class. It is worth noting that the procedure does not make any a-priori assumption on the attribution of the age as a function of the structural material, because in each census tract, for each structural material, we know exactly from ISTAT the number of buildings in each age class. Therefore, the only assumption made is that URM typologies are assigned to the oldest age classes first; the procedure moves to RC only once all URM buildings have been allocated. Moreover, the procedure assumes that the number of stories is statistically independent from the other taxonomic parameters (material and period). While RC structures generally tend to have more stories than masonry buildings, this is not always the case in Liguria, where many very tall masonry buildings are prevalent. Furthermore, the ISTAT 2011 data broadly classify the number of stories into categories such as 1, 2, 3, and 4 + stories, grouping buildings of varying heights into a single class. This broad classification, combined with the specific characteristics of the Ligurian building stock, implies that a direct correlation between material and average height is less straightforward in this area. The assumption regarding the distribution of the number of stories appears a reasonable choice for the Liguria region, based on the available data and local building typologies. However, the validity of this hypothesis must be carefully verified for any specific site of interest. Finally, the algorithm incorporates internal consistency checks. For instance, the sum of the disaggregated subtypologies should match the original aggregated ISTAT totals for each parameter (material, age of construction, number of storeys) at the census tract level. Indeed, small inconsistencies might occur due to rounding errors in the statistical distributions. The procedure was tested by comparing the disaggregated outputs with detailed in-situ survey data. Figure 10 provides this comparison for census tract 68, in which a building-by-building survey was conducted (Sect. 3.1). In particular, Fig. 10a compares the aggregated distributions of buildings by material, construction period, and number of storeys reported by ISTAT with those derived from the in-situ survey. For this section, the aggregated data from both sources are comparable, with only minor differences. Figure 10b, which focuses on masonry buildings, compares the number of buildings for different combinations of construction age and number of storeys obtained by the proposed procedure using ISTAT data (shown in blue) and the

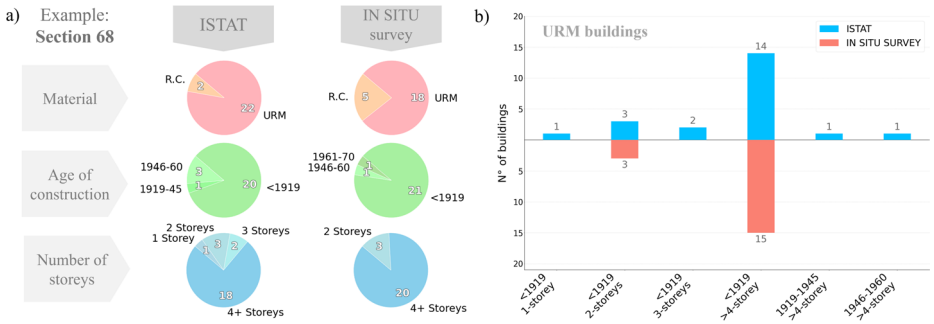

Fig. 10 Validation of the disaggregation procedure in census tract 68: (**a**) pie charts comparing aggregated distributions of buildings by material, age of construction, and number of storeys (ISTAT vs. in-situ survey) and (**b**) comparison of disaggregated ISTAT data (blue) against in-situ survey counts (red) for masonry buildings

in-situ survey (shown in red). The results are in good agreement, showing that the disaggregation procedure effectively captures both the dominant trends and the relative prevalence of different masonry sub-typologies (e.g., correctly identifying older masonry buildings as predominantly high-rise).

It is worth noting, however, that the reliability of the disaggregation results depends on the completeness and accuracy of the original ISTAT data. Inaccuracies can lead to sub-typology estimates that differ considerably from the actual building stock.

5 Results and sensitivity to hazard and exposure

This section presents and discusses the results from various damage scenarios generated for the Sanremo case study. As a reminder, all analyses are based on a deterministic ground-motion scenario for an earthquake compatible with the previously mentioned 23 February 1887 Ligurian Sea earthquake of magnitude 6.3 (see Sect. 3.2, Fig. 6a).

5.1 Impact of exposure data: ISTAT vs. in-situ surveys

As damage scenario accuracy depends heavily on exposure data quality, we compare standard ISTAT census data with detailed data from dedicated field surveys. To enable this comparison, we aggregated the building-specific field data for each of the thirty sections covered by the field survey. Figure 11 displays the difference between these two datasets (ISTAT vs. field survey) for each section, showing discrepancies in terms of the number of (a) total residential, (b) URM, and (c) RC buildings.

Differences in exposure are reflected in the damage estimates. The mean damage index μ_D is herein adopted as a metric for representing the overall physical impact on buildings within a scenario:

$$\mu_D = \sum_{k=0}^{5} p_k \cdot k \tag{2}$$

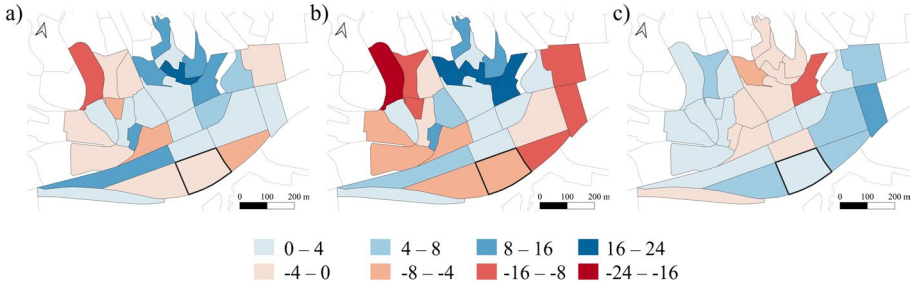

Fig. 11 Difference per census tract between ISTAT and in-situ survey building counts for (**a**) total buildings, (**b**) URM buildings, and (**c**) RC buildings. Red tones (negative differences) indicate that the number of buildings from field surveys are less than those from the ISTAT data, while blue tones (positive differences) represent the opposite case. The census tract outlined in black (section number 68) is the one analyzed in the previous paragraph (see Fig. 10)

where p_k, which can be determined from the given fragility curve, is the probability associated with each damage grade DS_k. The resulting index μ_D takes values between 0 (no damage) and 5 (collapse). Figure 12 compares, for the two exposure datasets (ISTAT vs. field survey) and for all census tracts shown in Fig. 11, the mean damage index μ_D values derived from the PGA scenario based on the amplification factor F_S used by the ITA18 attenuation model with $V_{s,30}$ values from Forte et al. (2019). Figure 12a (ISTAT) and Fig. 12b (field survey) compare the results for masonry buildings, Fig. 12c (ISTAT) and Fig. 12d (field survey) refer to RC buildings. The comparison reveals that, in about half of the census tracts, the use of field survey data results in higher values of μ_D, thus suggesting a potentially greater impact on the risk estimate. This holds for both URM and RC structural types.

5.2 Impact of fragility models and amplification factors

To investigate the sensitivity of the damage estimates to different modeling choices, we developed several scenarios by combining various site amplification factors (H) and fragility models (FM), indexed from Ha-FMa to Hd-FMc in Table 1. The scenario labelled as Hd-FMc, which we consider the reference scenario, refers to site amplification factors derived from specific MS studies (FA factors) and employs fragility curves from the DBV-Masonry model according to the *urban-* format applied at the sector level. The primary goal of this analysis is to quantify the impact of alternative input assumptions on the predicted consequences in terms of unsafe and collapsed buildings. Specifically, the analysis examines how the results change relative to the reference scenario when (i) only the site amplification factors are varied (Ha-FMc, Hb-FMc, and Hc-FMc), and (ii) only the fragility models are varied (Hd-FMa and Hd-FMb). It is worth noting that the sensitivity (and uncertainty) analysis only focuses on the hazard and vulnerability parameters. We did not include exposure in this analysis, as we opted to use only in-situ, building-by-building collected data.

The comparison focuses on the physical impact on the building stock, particularly the number of unusable and collapsed buildings. These outcomes are quantified by the number of buildings falling in each damage state (DS0 to DS5). Following standard procedures from

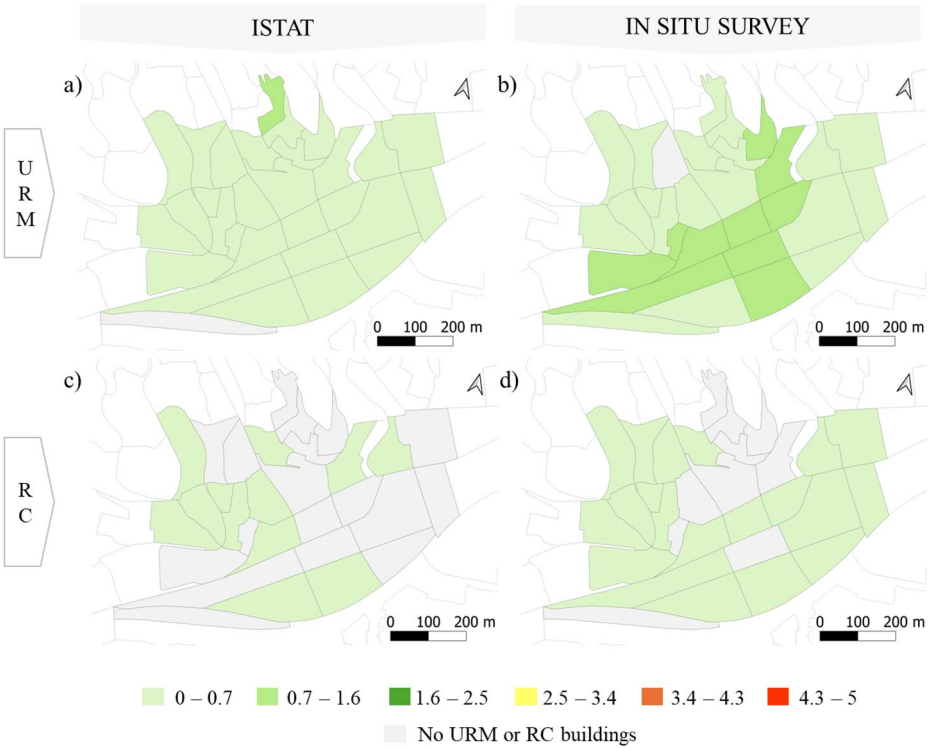

Fig. 12 Comparison of the mean damage index μ_D at the census tract scale: (**a**) URM buildings based on ISTAT data, (**b**) URM buildings from aggregated field survey data, (**c**) RC buildings based on ISTAT data, and (**d**) RC buildings from aggregated in-situ data

Table 1 Combinations of site amplification factors (H) and fragility models (FM) adopted to elaborate different damage scenarios. Scenario Hd-FMc represents the reference configuration

			H			
			a	b	c	d
			F_S (ITA18) Forte	F_S (ITA18) Mori	SS (NTC18) Forte	FA(MS)
FM	a	National Heuristic	Ha-FMa	Hb-FMa	Hc-FMa	Hd-FMa
	b	National DBV-Masonry	Ha-FMb	Hb-FMb	Hc-FMb	Hd-FMb
	c	Sector-specific DBV-Masonry	Ha-FMc	Hb-FMc	Hc-FMc	Hd-FMc

National Risk Assessment studies (Dolce et al., 2021), we translate this physical damage into other key impact metrics. First, we estimate the number of short-term unsafe buildings, which require immediate evacuation, by summing 40% of the buildings in DS2 and 40% in DS3. Next, we calculate the number of long-term unsafe buildings – those likely needing repair before re-occupancy – as 60% of buildings in DS3 plus those in DS4. Finally, the number of fully collapsed buildings is determined as all the buildings in DS5. Figure 13 provides a summary of the maximum number of unsafe short-term, unsafe long-term, and collapsed masonry buildings for each scenario in panel (a), where the highlighted cell identifies the reference scenario (Hd-FMc), for which the spatial distribution and number of

a)

FM-H	short-term unsafe URM buildings	long-term unsafe URM buildings	collapsed URM buildings
Ha-FMc	2.85	1.68	0.02
Hb-FMc	3.48	2.14	0.03
Hc-FMc	3.67	2.41	0.04
Hd-FMa	10.59	7.28	0.31
Hd-FMb	7.94	6.50	0.21
Hd-FMc	**9.10**	8.91	0.33

b)

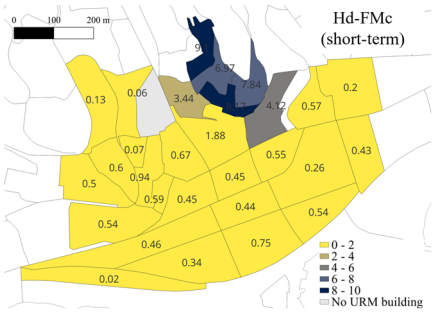

Fig. 13 (**a**) Summary of predicted damage to URM buildings, showing the number of unsafe and collapsed structures for each scenario in Table 1. The highlighted cell indicates the unsafe buildings visualized in Fig. 14, while the darker shading highlights the reference scenario (Hd-FMc). (**b**) Spatial distribution and number of short-term unsafe URM buildings for the reference scenario Hd-FMc

short-term unsafe URM buildings are shown in panel (b). Changing the input hazard (i.e., amplification factor), we find a significant difference in damage prediction. As expected, the scenarios using hazard inputs Ha, Hb, and Hc result in considerably fewer affected buildings than the reference scenario (Hd), which is based on site-specific factors from detailed MS studies that provide greater amplification. This consequently yields substantially greater damage estimates than the SS and F_S factors. Keeping the reference hazard input fixed (Hd) and varying the fragility model shows that the national heuristic model (FMa) is the most conservative, predicting the highest number of damaged buildings. On the other hand, the two DBV models produce similar results: the national model (FMb) predicts a slightly lower number of affected buildings than the reference sector-specific model (FMc), making the latter marginally more conservative.

Figure 14 shows the spatial distribution of damage, comparing the number of short-term unsafe buildings for each alternative scenario to those corresponding to the reference scenario (Hd-FMc), which consistently provides the most conservative (i.e., highest) estimate of damage. These comparisons are shown in Fig. 14a-e in terms of percentage differences over the total number of unsafe buildings of the tract. Figure 14f shows the spatial distribution of the CARTIS building sectors across the 30 census tracts analyzed. This map indicates which fragility curve, derived from the DBV-Masonry method, was assigned to each area for the scenario analysis. The colours correspond directly to the fragility curves plotted in Fig. 9. Again, the influence of the hazard input is significant (Fig. 14a-c). The FA(MS) site amplification factor used in the reference scenario (Hd-FMc) yields substantially higher damage predictions than the SS and F_S factors used in the alternative evaluations. These differences are often large, demonstrating that the choice of amplification factor has a strong effect on the final scenario. Varying the fragility models also produces differences, although they are generally less pronounced (Fig. 14d-e). Both the Heuristic (FMa) and DBV-National (FMb) models result in lower damage estimates than the reference sector-specific model (FMc), with the DBV-National model providing results that, except for some areas, are closer to the reference (Fig. 14e). In conclusion, in our application, the site amplification factor appears to have a predominant influence on the results. However, the combined contribution of these

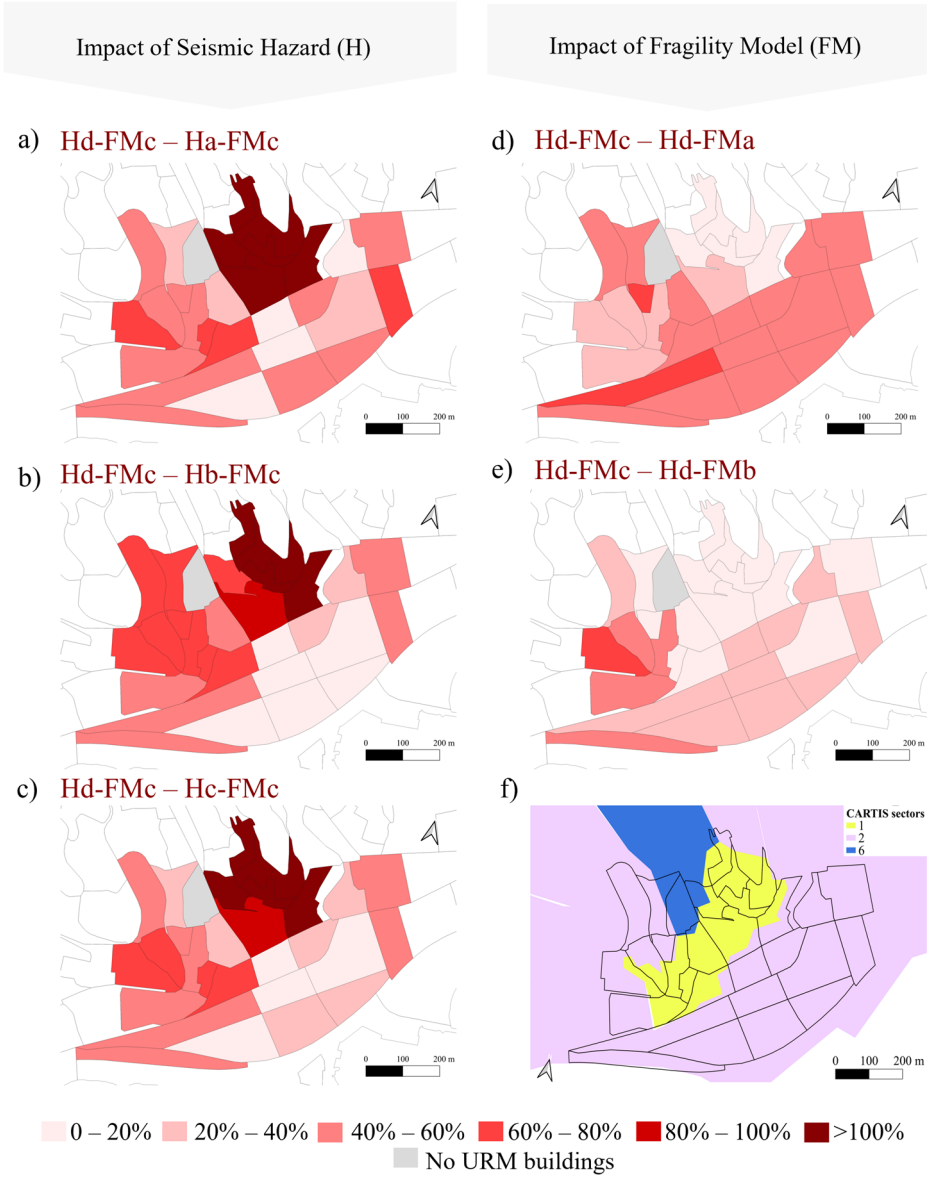

Fig. 14 (**a** to **e**) Maps showing the percentage difference of short-term unsafe masonry buildings for each alternative scenario (Table 1) relative to the reference Hd-FMc scenario, whose sector-specific fragility model (DBV-Masonry) is spatially defined by the CARTIS sectors shown in panel (**f**), and which incorporates the FA(MS) site amplification factor

two components is complex and location-dependent, precluding generalizations across the entire study area or to other case studies.

6 Conclusions

This study investigated and quantified how the level of detail in input data influences seismic damage scenarios at the urban scale through a multi-level comparative framework. Specifically, we focused on the impact of various data sources that describe earthquake hazard and building vulnerability. The application to the municipality of Sanremo, in northwestern Italy, demonstrated the importance of incorporating detailed local information into damage assessments. Although the moderate seismicity of the area leads to limited expected consequences, from a methodological standpoint, the study showed that variations in data quality exert a considerable impact. A key finding is that scenarios created using site-specific data, such as local soil conditions and vulnerability models based on detailed field surveys, can differ significantly from those relying solely on generic, national-scale information, like standard soil maps and census-based building data.

The analysis highlighted that the choice of both vulnerability models and methods to quantify site amplification strongly impacts the predicted spatial distribution and intensity of damage. Furthermore, a comparison between standard census data and data from detailed on-site surveys revealed significant differences in the characterization of building features, leading to considerable variations in key outcomes, such as the number of unsafe or collapsed structures. The sensitivity analysis demonstrates that the multi-level approach effectively captures the variability of potential damage outcomes. This capability offers a strategic advantage for two key purposes: emergency response and long-term planning. A key strength of the procedure is its ability to combine readily available national data with more refined local information. In the critical post-earthquake hours, understanding the possible range of damage consequences is crucial for enhancing situational awareness. The thematic maps of expected damage presented in the paper, which can be made accessible and interactive via a Web-GIS platform, could be further integrated with socio-economic impact models, providing preliminary estimates of the consequences of structural damage and collapse, such as the number of people affected and critical road closures. This would provide a synoptic, rapid, yet spatially defined overview of the expected earthquake consequences, thus allowing the identification of the most affected areas, the definition of priorities for rescue operations and planning of on-site damage and safety assessments, and a more rational and efficient allocation of available resources during the first hours following a destructive seismic event. Beyond immediate crisis response, the findings of the study are also highly valuable for long-term risk management and mitigation planning by local governments. Through detailed maps of potential damage, municipal authorities can obtain critical insights into a city's seismic vulnerabilities. This information facilitates identifying the most critical areas, interconnections, or building types needing further investigation, targeted seismic retrofitting programs, or better resource allocation for risk reduction.

A primary future challenge is to accurately classify building types by exploiting advanced approaches, such as machine learning. Adopting these methods as an alternative to the simple algorithm used in this work to interpret census parameters (material, age, and number of storeys) could enhance the reliability of exposure models derived from basic

census information. Another key area for improvement is the incorporation of real-time data from dense monitoring networks. Future work will focus on integrating live ground motion data to rapidly update the initial hazard scenario, moving from purely predictive maps to assessments constrained by real-world observations. Moreover, direct measurements of building response during an earthquake could provide a factual basis for validating or even refining the adopted vulnerability models in near-real time, thereby increasing confidence in the predicted damage for similar building types. Finally, a crucial future development is the systematic quantification of epistemic uncertainties. The methodology could integrate multiple plausible assumptions regarding the choice of the most appropriate models and parameters. This includes uncertainty in ground motion prediction, stemming from the intrinsic variability of the chosen GMPE, uncertainty in site amplification, arising from the choice between different methods (e.g., period-dependent local factors versus simplified code-based approaches), and the uncertainty associated with vulnerability functions, deriving from the adoption of different fragility models (e.g., mechanical versus empirical) and the dispersion within the curves themselves. In conclusion, this work demonstrates that the detail and source of input data are not minor variables but critical drivers of urban seismic damage assessments, highlighting the necessity of a multi-level approach to understand and bracket the potential range of outcomes. Communicating this range of outcomes, rather than a single deterministic scenario, is paramount for informed decision-making, as it provides end-users with a clearer understanding of the confidence level of the damage predictions and is essential for robust post-earthquake planning and risk mitigation.

Supplementary Information The online version contains supplementary material available at https://doi.org/10.1007/s10518-026-02371-6.

Acknowledgements This work was supported by the European Union - NextGenerationEU and by the Ministry of University and Research (MUR), National Recovery and Resilience Plan (NRRP), Mission 4, Component 2, Investment 1.5, project "RAISE -Robotics and AI for Socio-economic Empowerment" (ECS00000035). Serena Cattari is part of RAISE Innovation Ecosystem. This work also benefited from the contribution of Eng. Sara Alfano and the support of the RETURN Foundation, particularly for the analyses described in Sect. 4.3. Thanks are extended to Regione Liguria for making available the seismic microzonation studies conducted for the Municipality of Sanremo.

Author contributions MGBM: conceptualization, methodology, formal analysis and investigation, data curation, software, validation, visualization, writing – original draft preparation; DS: conceptualization, methodology, software, supervision, writing – review and editing; SL: software, writing – review and editing; SB: conceptualization, methodology, supervision, funding acquisition, resources, writing – review and editing; SC: conceptualization, methodology, supervision, funding acquisition, resources, writing – review and editing. All authors read and approved the final manuscript.

Funding Open access funding provided by Università degli Studi di Genova within the CRUI-CARE Agreement. Funded by the European Union - NextGenerationEU and by the Ministry of University and Research (MUR), National Recovery and Resilience Plan (NRRP), Mission 4, Component 2, Investment 1.5, project "RAISE -Robotics and AI for Socio-economic Empowerment" (ECS00000035).

Data availability All data used in this research are publicly available from the sources listed below. *Seismic network data:* The system's data processing chain is designed to integrate information from national and regional monitoring networks, including the Italian Seismic Network (RSN), managed by the National Institute of Geophysics and Volcanology (INGV) [Istituto Nazionale di Geofisica e Vulcanologia (INGV). (2005). Rete Sismica Nazionale (RSN) [Data set]. Istituto Nazionale di Geofisica e Vulcanologia (INGV). https://doi.org/10.13127/SD/X0FXNH7QFY], and the Regional Seismic Network of Northwestern Italy (RSNI) of the University of Genoa [https://doi.org/10.7914/SN/GU]. *Building exposure data:* The building exposure model was developed using aggregated data from the 2011 Italian census, provided by the Italian National

Institute of Statistics (ISTAT), with the disaggregation procedure detailed in the Methodology section. This dataset, along with others generated during the study, is available from the corresponding author on reasonable request. *Software and tools:* The development of damage scenarios and all related data processing were conducted using custom scripts written by the authors in Python (Python Software Foundation. Python Language Reference, version 3.11 available at http://www.python.org). Geospatial analysis and the generation of map figures (Figs. 3, 5, 11, 12 and 14) were performed using QGIS software (version 3.34.9-Prizren, which can be downloaded at https://qgis.org).

Declarations

Competing interests The authors have no relevant financial or non-financial interests to disclose.

References

Adhikari RK, D'Ayala D, Fernandez R, Yamin L, Nassirpour A, Vatteri AP, Cortes F (2023) GLOSI taxonomy: A tool for 'seismic risk assessment' oriented classification of school buildings. Int J Disaster Risk Reduct 87:103594

Alexander DE (2010) The l'aquila earthquake of 6 April 2009 and Italian government policy on disaster response. J Nat Resour Policy Res 2(4):325–342

Barani S, Spallarossa D, Bazzurro P, Eva C (2007) Sensitivity analysis of seismic hazard for Western Liguria (North Western Italy): a first attempt towards the Understanding and quantification of hazard uncertainty. Tectonophysics 435(1–4):13–35

Barani S, Ferretti G, De Ferrari R (2020) Incorporating results from seismic microzonation into probabilistic seismic hazard analysis: an example in western Liguria (Italy). Eng Geol 267:105479

Bilham R (2009) The seismic future of cities. Bull Earthq Eng 7(4):839–887

Borzi B, Onida M, Faravelli M, Polli D, Pagano M, Quaroni D, Moroni C (2021) IRMA platform for the calculation of damages and risks of Italian residential buildings. Bull Earthq Eng 19:3033–3055

Brando G, Cianchino G, Rapone D, Spacone E, Biondi S (2021) A CARTIS-based method for the rapid seismic vulnerability assessment of minor Italian historical centres. Int J Disaster Risk Reduct 63:102478

Brunelli A, de Silva F, Cattari S (2022) Observed and simulated urban-scale seismic damage of masonry buildings in aggregate on soft soil: the case of visso hit by the 2016/2017 central Italy earthquake. Int J Disaster Risk Reduct 83:103391

Brzev S, Scawthorn C, Charleson AW, Allen L, Greene M, Jaiswal K, Silva V (2013) GEM Building taxonomy (Version 2.0). GEM Foundation. No. 2013-02

Carpanese P, Donà M (2023) Automatic identification of residential Building features using machine learning techniques. Procedia Struct Integr 44:1980–1987

Cattari S, Ottonelli D, Mohammadi S (2024) EQ-DIRECTION procedure towards an improved urban seismic resilience: application to the pilot case study of Sanremo municipality. Sustainability 16(6):2501

Chieffo N, ELCmenti F, Formisano A, Lenci S (2019) Comparative fragility methods for seismic assessment of masonry buildings located in muccia (Italy). J Building Eng 25:100813

Chieffo N, Formisano A, Miguel Ferreira T (2021) Damage scenario-based approach and retrofitting strategies for seismic risk mitigation: an application to the historical centre of sant'antimo (Italy). Eur J Environ Civil Eng 25(11):1929–1948

Chirico A, Corsanego A, Giorgini G, Roggeri G, Ugolini P (1992) Recupero vulnerabilità e Rischio Sismico Nei centri storici Della Liguria. Il caso La Pigna di Sanremo

da Porto F, Donà M, Rosti A, Rota M, Lagomarsino S, Cattari S, Speranza E (2021) Comparative analysis of the fragility curves for Italian residential masonry and RC buildings. Bull Earthq Eng 19(8):3209–3252.

Dipartimento della protezione civile (2014) Manuale per l'analisi della Condizione Limite per l'Emergenza (ELC) dell'insediamento urbano. Versione 1.0

Dolce M (2012 Sep) The Italian national seismic prevention program. In 15th World Conference on Earthquake Engineering. Retrieved from: http://www.civil.ist.utl.pt/~mlopes/conteudos/SISMOS/DOLCE.pdf

Dolce M, Speranza E, Giordano F, Borzi B, Bocchi F, Conte C, Pascale V (2019) Observed damage database of past Italian earthquakes: the Da. DO WebGIS. Bollettino di Geofisica Teorica ed Applicata, 60(2)

Dolce M, Prota A, Borzi B, da Porto F, Lagomarsino S, Magenes G, Zuccaro G (2021) Seismic risk assessment of residential buildings in Italy. Bull Earthq Eng 19:2999–3032

Dolce M, Speranza E, Bocchi F, Conte C (2018) Probabilistic assessment of structural operational efficiency in emergency limit conditions: the I. OPà. ELC method. Bull Earthq Eng 16(9):3791–3818

Faenza L, Michelini A (2010) Regression analysis of MCS intensity and ground motion parameters in Italy and its application in shakemap. Geophys J Int 180(3):1138–1152

Ferreira TM, Maio R, Vicente R (2017) Seismic vulnerability assessment of the old City centre of Horta, azores: calibration and application of a seismic vulnerability index method. Bull Earthq Eng 15:2879–2899

Forte G, Chioccarelli E, De Falco M, Cito P, Santo A, Iervolino I (2019) Seismic soil classification of Italy based on surface geology and shear-wave velocity measurements. Soil Dyn Earthq Eng 122:79–93

Freeman SA (1998), September The capacity spectrum method as a tool for seismic design. In Proceedings of the 11th European conference on earthquake engineering (pp. 6–11). France: Paris

Gouveia F, Silva V, Lopes J, Moreira RS, Torres JM, Simas Guerreiro M (2024) Automated identification of Building features with deep learning for risk analysis. Discover Appl Sci 6(9):466

Grunthal G (ed) (1998) European Macroseismic Scale 1998 (EMS-98). Cahiers du Centre Européen de Géodynamique et de Séismologie, Vol. 15, Luxembourg

Ilic JM, Bento R, Cattari S (2020) 3DGIS representation for supporting seismic mitigation policies at urban scale: the case study of Lisbon. J Cult Herit 45:265–278

Istituto Nazionale di Geofisica e Vulcanologia (INGV) (2005) Rete Sismica Nazionale (RSN) [Data set]. Istituto Nazionale di Geofisica e Vulcanologia (INGV). https://doi.org/10.13127/SD/X0FXNH7QFY

Kircher CA, Whitman RV, Holmes WT (2006) HAZUS earthquake loss Estimation methods. Nat Hazards Rev 7(2):45–59

Kohrangi M, Vamvatsikos D, Bazzurro P (2016) Implications of intensity measure selection for seismic loss assessment of 3-D buildings. Earthq Spectra 32(4):2167–2189

Lagomarsino S, Cattari S (2013) Fragility functions of masonry buildings. SYNER-G: typology definition and fragility functions for physical elements at seismic risk: buildings, lifelines, transportation networks and critical facilities. Springer Netherlands, Dordrecht, pp 111–156

Lagomarsino S, Giovinazzi S (2006) Macroseismic and mechanical models for the vulnerability and damage assessment of current buildings. Bull Earthq Eng 4:415–443

Lagomarsino S, Masi A (2022) Mappe di rischio sismico dell'edilizia residenziale. Final Report WP4-MARS, DPC-ReLUIS Project 2019–2021. ReLUIS, Naples. Available (in Italian) at: https://www.reluis.it/wp-content/uploads/2024/01/Report-WP4-MARS-residenziale_19-21.pdf. Accessed 02 December 2025

Lagomarsino S, Cattari S, Ottonelli D (2021) The heuristic vulnerability model: fragility curves for masonry buildings. Bull Earthq Eng 19:3129–3163

Lanzano G, Luzi L, Pacor F, Felicetta C, Puglia R, Sgobba S, D'Amico M (2019) A revised ground-motion prediction model for shallow crustal earthquakes in Italy. Bull Seismol Soc Am 109(2):525–540

Li S, Li C, Huang Y, Zhai C (2024) Real-time seismic damage simulation for urban Building portfolio based on basic Building information and machine learning. Int J Disaster Risk Reduct 111:104687

Ministero delle Infrastrutture e dei Trasporti (2018) Norme tecniche per Le costruzioni. Decreto Del Ministero Delle Infrastrutture GU serie generale(42):20022018–Supplordinario8. https://www.gazzettaufficiale.it/eli/id/2023/03/22/23A01847/SG Gazzetta ufficiale della Repubblica Italiana

Mori F, Mendicelli A, Moscatelli M, Romagnoli G, Peronace E, Naso G (2020) A new Vs30 map for Italy based on the seismic microzonation dataset. Eng Geol 275:105745

Oliveti I, Faenza L, Michelini A (2022) New reversible relationships between ground motion parameters and macroseismic intensity for Italy and their application in shakemap. Geophys J Int 231(2):1117–1137

Pitilakis K, Crowley H, Kaynia AM (2014) SYNER-G: typology definition and fragility functions for physical elements at seismic risk. Geotech Geol Earthq Eng 27:1–28

Polese M, d'Aragona MG, Prota A (2019) Simplified approach for Building inventory and seismic damage assessment at the territorial scale: an application for a town in Southern Italy. Soil Dyn Earthq Eng 121:405–420

Rovida A, Locati M, Camassi R, Lolli B, Gasperini P, Antonucci A (2022) Catalogo parametrico dei terremoti italiani (cpti15). INGV versione, 4

Silva V, Crowley H, Pagani M, Monelli D, Pinho R (2014) Development of the openquake engine, the global earthquake model's open-source software for seismic risk assessment. Nat Hazards 72:1409–1427
Silva V, Yepes-Estrada C, Dabbeek J, Martins L, Brzev S (2018) GED4ALL-Global exposure database for multi-hazard risk analysis–multi-hazard exposure taxonomy. Global Earthquake Model Foundation: Pavia, Italy
Tocchi G, Polese M, Prota A (2023) Improving Building inventory with a machine learning approach: application in Southern Italy. Procedia Struct Integr 44:1972–1979
University of Genoa (1967) Regional seismic network of North Western Italy [Dataset]. https://doi.org/10.7914/SN/GU. International Federation of Digital Seismograph Networks
Vicente R, Parodi S, Lagomarsino S, Varum H, Silva JM (2011) Seismic vulnerability and risk assessment: case study of the historic City centre of Coimbra, Portugal. Bull Earthq Eng 9:1067–1096
Wald DJ, Quitoriano V, Heaton TH, Kanamori H, Scrivner CW, Worden CB (1999) TriNet shakemaps: rapid generation of peak ground motion and intensity maps for earthquakes in Southern California. Earthq Spectra 15(3):537–555
Zhang G, Liu K, Wen W, Zhai C, Zhang C, Zhou B (2025) Rapid seismic damage assessment of Building portfolio based on fusion of surrogate model and monitored data. Int J Disaster Risk Reduct 119:105293
Zuccaro G, Dolce M, Perelli FL, De Gregorio D, Speranza E (2023) CARTIS: a method for the typological-structural characterization of Italian ordinary buildings in urban areas. Front Built Environ 9:1129176

Authors and Affiliations

Margherita Gabriella Bruna Merani[1] · Daniele Sivori[1,3] · Sergio Lagomarsino[1] · Simone Barani[2] · Serena Cattari[1]

✉ Margherita Gabriella Bruna Merani
margherita.merani@edu.unige.it

[1] Department of Civil, Chemical and Environmental Engineering (DICCA), University of Genoa, Via Montallegro 1, 16145 Genoa, Italy

[2] Department of Earth, Environmental and Life Sciences (DISTAV), University of Genoa, Corso Europa 26, 16132 Genoa, Italy

[3] Present address: Centre for Training and Research on Reduction of Seismic Risk (ROSE Centre), Scuola Universitaria Superiore IUSS Pavia, Palazzo del Broletto, Piazza della Vittoria 15, 27100 Pavia, Italy